INTERNATIONAL JOURNAL OF REMOTE SENSING, 2016
http://dx.doi.org/10.1080/01431161.2016.1264028

Determining tree height and crown diameter from high-resolution UAV imagery

Dimitrios Panagiotidis, Azadeh Abdollahnejad, Peter Surový and Vasco Chiteculo

Department of Forest Management, Czech University of Life Sciences, Prague, Czech Republic

ABSTRACT

Advances in computer vision and the parallel development of unmanned aerial vehicles (UAVs) allow for the extensive use of UAV in forest inventory and in indirect measurements of tree features. We used UAV-sensed high-resolution imagery through photogrammetry and Structure from Motion (SfM) to estimate tree heights and crown diameters. We reconstructed 3D structures from 2D image sequences for two study areas (25 × 25 m). Species composition for Plot 1 included Norway spruce (*Picea abies* L.) together with European larch (*Larix decidua* Mill.) and Scots pine (*Pinus sylvestris* L.), whereas Plot 2 was mainly Norway spruce and Scots pine together with scattered individuals of European larch and Silver birch *(Betula pendula* Roth.). The involved workflow used canopy height models (CHMs) for the extraction of height, the smoothing of raster images for the determination of the local maxima, and Inverse Watershed Segmentation (IWS) for the estimation of the crown diameters with the help of a geographical information system (GIS). Finally, we validated the accuracies of the two methods by comparing the UAV results with ground measurements. The results showed higher agreement between field and remote-sensed data for heights than for crown diameters based on RMSE%, which were in the range 11.42–12.62 for height and 14.29–18.56 for crown diameter. Overall, the accuracy of the results was acceptable and showed that the methods were feasible for detecting tree heights and crown diameter.

ARTICLE HISTORY
Received 8 July 2016
Accepted 5 November 2016

1. Introduction

The determination of tree height is important, mainly because of biological and commercial reasons. It is a significant indicator, reflecting a site's productive capacity of the species concerned, when it is growing on a particular site. Site productive capacity means the total stand biomass produced by a stand on a particular site, up to any particular stage of its development, when the stand has been using fully the resources necessary for tree growth, which are available from the site. Furthermore, it is height, rather than biomass, that best reflects the site productive capacity (Shao, Zhao, and Shugart 1996).

CONTACT Dimitrios Panagiotidis panagiotidis@fld.czu.cz Department of Forest Management, Czech University of Life Sciences, Prague, Czech Republic

Similarly, tree crown size has been shown to be a multipurpose ecological indicator. It determines, among others, carbon sequestration, shading, risk of wind-breakage, and tree growth. The dependence of crown size on resource supply, species, and tree age complicates an accurate evaluation of a tree's space requirement, and its size-dependent functions and services in forested areas. Many remote-sensing applications involve the estimation of individual tree canopy area (Kalliovirta and Tokola 2005), as an intermediate stage in differentiating the signals reflected from the forest canopy and the forest floor, e.g. estimation of timber volume (Bolduc et al. 1999; Maltamo et al. 2004). Forest canopy height is an important structural parameter in several forest inventories; very-high-resolution digital models have been developed to identify and quantify individual tree crowns separately using remote technology. A digital elevation model (DEM) or a digital terrain model (DTM) is used for bare ground modelling without considering the features on the ground surface (Peckham and Gyozo 2007). On the other hand, digital surface models (DSMs) consider the features on the ground surface, e.g. trees and buildings. Methods used to generate DSMs usually focus on photogrammetric methods. However, this technique requires a well-trained workforce, high-quality digital cameras, and precise technology that will ensure the integrity of the data for accurate results. Several examples of the retrieval of canopy height using multi-angle/multi-view passive imagery from airborne platforms exist (Waser et al. 2008). Emerging techniques of computer vision in parallel with the recent advances of unmanned aerial systems (UASs) enable the extraction of reliable 2D and 3D imagery information from the collection of multi-angle imagery analysis taken with standard (non-metric) cameras and derived by Structure from Motion (SfM) algorithms (Küng et al. 2011; James and Robson 2012). These developments have made it possible to construct dense point clouds based on feature matches (alignment) within a series of overlapping photographs, even if internal and external camera orientation parameters are not available (Turner, Lucieer, and Watson 2012). New methods of photograph reconstruction enable the generation of very-high-resolution DSMs and orthophotograph mosaics with high spatial resolution (Turner, Lucieer, and Watson 2012; Fritz, Kattenborn, and Koch 2013; Dandois and Ellis 2013; Gini et al. 2014; Sona et al. 2014), and they have been used for environmental monitoring (Diaz Varela et al. 2014) and quantifying tree heights and crown dimensions (Zarco-Tejada et al. 2014). Several studies have identified the potential of combining UAV image flights and the SfM processing chain for terrain modelling (Remondino et al. 2011; Dandois and Ellis 2013), in terms of runtime and accuracy, as well as visual appearance of the resulting reconstructions.

A canopy height model (CHM) represents the difference between the top canopy surface and the underlying ground topography, i.e. subtraction of DSM from DTM. Popescu (2007) proposed that a CHM could be described as a 3D surface that contains all the necessary information about vegetation height above ground surface. The CHM can be effectively derived from digital image raw data through the appropriate filtering/classification of photograph point clouds to distinguish ground and canopy points; this separation can be achieved using various software, such as LasTools and Agisoft PhotoScan ©, and the latter is equipped with a tool for automatic and manual ground point classification (Agisoft). CHMs are raster images that allow us to delineate individual tree crowns and detect treetops. Individual tree identification (ITD) based on the CHM can be performed with a range of algorithms and procedures, including image smoothing, local maxima finding, and template matching (Persson, Holmgren, and Soderman

2002; Popescu, Wynne, and Nelson 2002; Koch, Heyder, and Weinacker 2006; Chen et al. 2006; Falkowski et al. 2006). By identifying the individual tree positions based on smoothing and local maxima filtering, tree height can be directly measured from CHMs using regression models (Pyysalo and Hyyppä 2002; Popescu, Wynne, and Nelson 2003).

Watershed segmentation is an important member of the boundary detection-based segmentation family (Carleer, Debeir, and Wolff 2005). Additionally, it is the most popular technique used for segmenting a CHM, because it is intuitive to treat each concave tree crown in the inverted CHM as a catchment basin. The surface of the raster is segmented into the equivalent of individual drainage basins by identifying local maximum and nearest minima values. Based on this approach, Inverse Watershed Segmentation (IWS) can delineate distinct tree entities with height values and crown diameters (Edson and Wing 2011). The method assumes that local maxima present in the CHM are treetops; however, caution should be exercised when applying local maxima in structurally complex forest structures. For example, multiple local maxima are often identified within a single broadleaf crown because of the irregularity of crowns and, in part, from random errors associated with the creation of the CHM. A possible solution is the use of smoothing filters when constructing the CHM; however, caution is required because strong filters may eliminate smaller trees. Popescu, Wynne, and Nelson (2003) suggested an improved version of local maxima filtering using a locally variable window size relative to tree height by referring to a predefined height-crown equation that accounts for tree crown development related to tree growth. However, other studies have reported problems correctly identifying tree crowns using a tree-level approach, particularly in closed-canopy and denser forests. According to Wang, Gong, and Biging (2004), the assumption that treetops are located around the vicinity of the centre of a crown can be met only when the view area is within ±15° of nadir. This assumption may not be applicable to trees located outside of this range because treetops lean away from the nadir point. Moreover, for trees viewed from outside of the near-nadir direction, the silhouettes detected from the edge-detection methods are inconsistent with the real tree crown boundaries, whereby trees are often misidentified or even missing in some cases.

The number and quality of algorithms are increasing rapidly. Sophisticated algorithms, such as IWS, are designed to consider increasingly more aspects, in either the preprocessing or post-processing of images, in an attempt to minimize oversight errors and provide a friendlier processing environment for the analyst. Delineation of individual trees is a complex process and sometimes an acceptable algorithm does not exist, even when using systems such as human vision, which is currently considered the most advanced image-processing tool. Bortolot (2006) investigated the practical advantages of using CHMs and proposed the use of CHM for identifying clusters of trees, which would correspond to a group of tree crowns for easier post-processing.

The key contribution of this article was to test the performance of photogrammetric techniques for the estimation of tree heights and crown diameters, based on UAV (DJI S800) SfM point clouds. We assessed the accuracy of height and crown diameter measurements derived from point clouds compared with ground measurements.

2. Materials and methods

2.1. *Study area and experimental design*

Two research plots from the Czech Republic (see Figure 1) were included in this work; Plot 1 is located southeast of Prague (N50.01577, E14.75998) and Plot 2 is located south of the city (N49.81452, E14.700590). Both plots were located on flat terrain and were 625 m^2 (25 X 25 m) in size. Plot 1 had 48 trees with predominantly Norway spruce (*Picea abies* L.*)*, with a few European larch (*Larix decidua* Mill.) and Scots pine (*Pinus sylvestris* L.) individuals scattered throughout. Plot 2 had 39 trees with mainly Norway spruce and Scots pine trees, with scattered individuals of European larch and Silver birch *(Betula pendula* Roth.). We measured all trees on each plot to estimate tree heights and crown diameters.

2.2. *Analysis overview*

An illustration of the methodology is summarized in Figure 2. Images were acquired using a Sony NEX-5 R digital camera, embedded on a UAV platform DJI S800 to create 3D reconstruction models for both study areas. The images were processed and analysed in Agisoft PhotoScan© to derive the DSM and DTM for both plots, using the SfM approach. The reconstructed mesh surface was derived from the point cloud by using

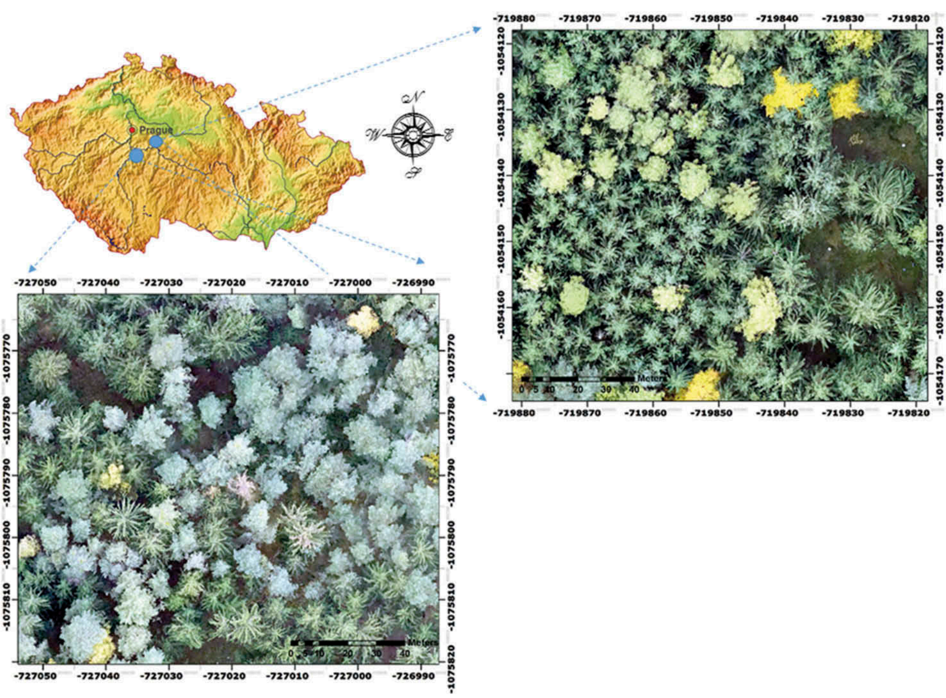

Figure 1. Plot locations in the Czech Republic. The top right photograph displays Plot 1 and the bottom left photograph displays Plot 2. Image sources: images provided as captured and post-processed from an RGB high-resolution embedded UAV camera using ESRI Inc. Map of the Czech Republic is from http://www.mapcruzin.com/free-czech-republicmaps (assessed on January 2016).

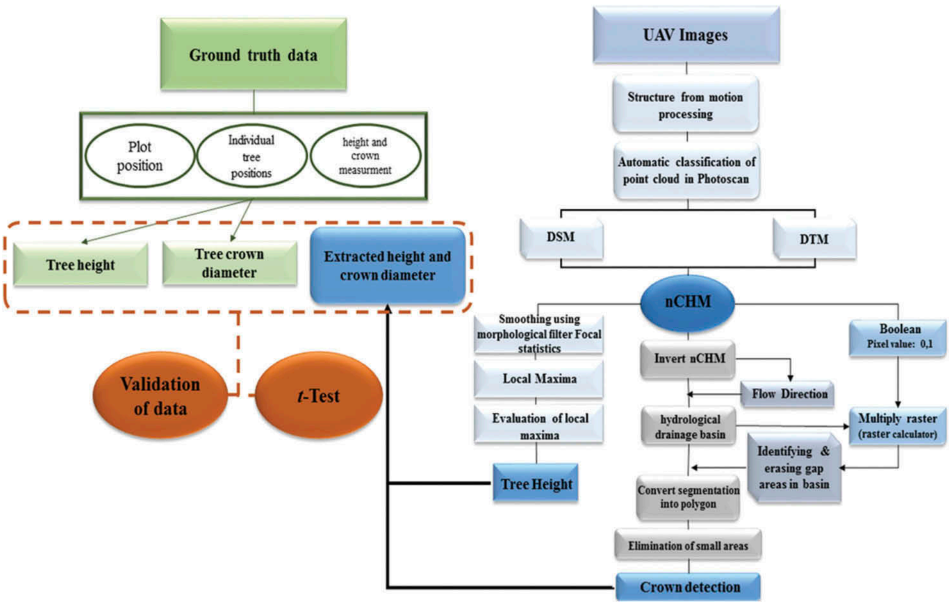

Figure 2. A flow chart to illustrate the analysis and outputs; the main objectives are in the shaded nodes.

the automatic classification of points procedure, based on three parameters: a) max angle, b) max distance, and c) cell size. To increase the accuracy of the resultant DSM and DTM models, we placed four ground control points (GCPs) in the corners of each square plot and we measured them with geodetic Real Time Kinematic (RTK) GPS. ArcGIS 10.3.1 by ESRI was used to create CHMs, from the difference in elevation between DSM and DTM (i.e. CHM = DSM − DTM). To estimate the tree heights, we used local maxima filtering, and for the crown diameters we used IWS in both study areas. Finally, statistical paired *t*-tests analyses were performed on the estimated and measured variables for both plots in order to evaluate the performance of the remote-sensing approach based on UAV SfM point clouds.

2.3. *Field measurements*

Tree heights were recorded using a TruPulse 360 /B laser range finder. To minimize height evaluation errors, the horizontal distance from the objective tree was at least equal to the tree height to be measured. We also measured the width of horizontal tree crown projections (east–west and north–south) for each tree using the TruPulse 360 /B laser range finder. We measured the positions of plot trees using the azimuth–distance approach from the plot centre, which was determined using RTK GPS Trimble Juno 3D handheld equipment; azimuth was estimated using a handheld compass and tree distance from plot centre was estimated using a Vertex III and Transponder T3 (Haglöf Sweden, 2002). We also created an index of the tree species for all measured trees. All field measurements for both plots were collected in the same month as the aerial images were taken.

2.4. *Photograph acquisition and 3D model reconstruction*

The DJI S800 UAV platform carried an RGB camera (see Figure 3). The camera was a Sony NEX-5R, with a 16 MP resolution and 4912 × 3264 pixels. The camera was mounted with a Voigtlander Super Wide Heliar lens, with a focal length of 15 mm. A drone needed approximately 7 min to complete a flight based on the predefined parameters (i.e. number of waypoints and time of flight), which we set using the DJI ground station software. A point cloud of images comprising the flight path lines covered the entire study area (see Figure 4). We performed all six flights, three flights per plot, in three different elevations using the same parameters, i.e. flight path pattern and altitudes.

The SfM image reconstruction process resulted in 673 of the original 718 images aligned in Plot 1 and 457 of the original 480 images aligned in Plot 2. We extracted both

Figure 3. This is a scaled image that illustrates the actual size of the multirotor UAV (DJI S800) that was used for photograph acquisition (source: Přemysl Janata).

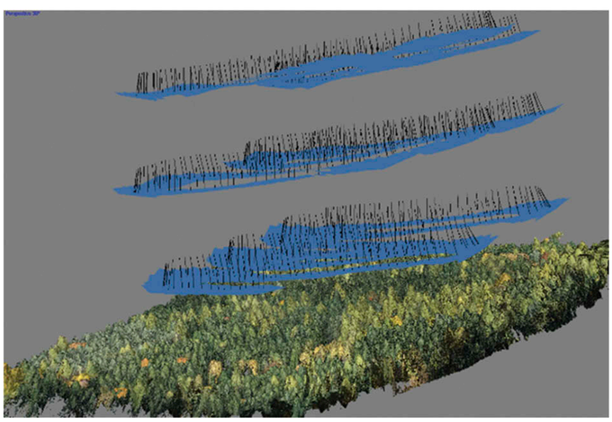

Figure 4. Flight performance for image acquisition at three different elevations (Plot 1, autopilot mode).

DSM and DTM (0.05 x 0.05 m cell size) as constructed from the total amount of aligned images for each plot using Agisoft PhotoScan©. We initially reconstructed the DTM mesh using automatic classification, based on classified sparse point clouds of the ground (as opposed to the construction of the DSM, which was based on the complete dense point cloud). The automatic classification was based on three parameters: i) maximum angle (deg), ii) max distance (m), and iii) cell size (m). In addition to the extraction of DSM and DTM, we located four reference points for each plot. GCPs distributed within the study areas (mainly at larger gap areas), measured with geodetic RTK GPS with centimetre accuracy, whereas the coordinate system was set to S-JTSK/Krovak East North (a local coordinate system that is mainly used in the Czech Republic).

The imagery and the synchronized on-board GPS position for each single image were used as input for image positions. During the alignment process, when the algorithm is trying to find and match points between overlapping images and refine the image positions for each photograph separately, we set the accuracy to high.

2.5. *Calculation of tree heights*

The setting parameters for local maxima were determined using the morphological filter-focal statistics tool in ArcGIS. This morphological filter is preferred when we need to identify the highest pixel value on the treetop from the CHM; therefore, it can be used to eliminate the possibility of having multiple local maxima within a single crown area. For individual tree position detection from the UAV platform, we used the adaptive filtering method based on CHM height values. In this method, an image-smoothing step was applied to the CHMs using low-pass filters to reduce the noise effect and regulate the values of the smoothing window as a stepwise function of the heights of the CHM (Dralle and Rudemo 1996; Pitkänen et al. 2004). Tree height was derived from the CHM based on the evaluation of local maxima, which were considered to be treetops (Figure 5(*a*)). The CHM was calculated by subtracting the DSM from the DTM using ArcGIS 10.3.1 by ESRI ©. This decision is usually based on the particular geometry of the forest structure and the spatial pattern of the targeted trees. Prior to any further calculations, and depending on the structure of tree crowns and resolution, values

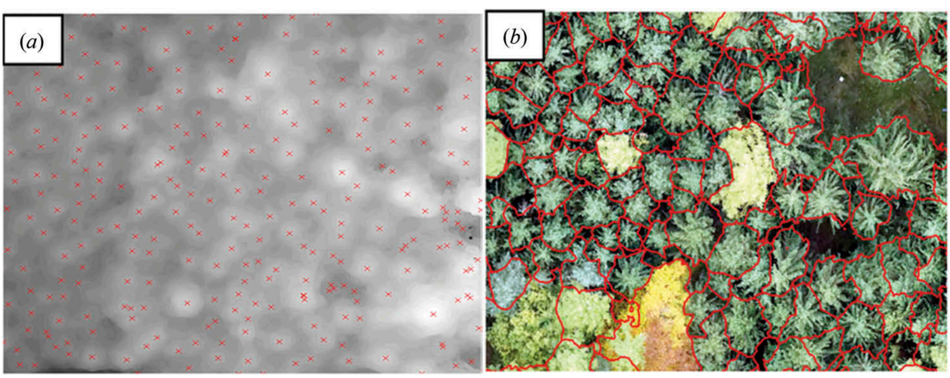

Figure 5. Example to illustrate (a) local maxima seeds identified as tree tops, and (b) tree crowns derived from the process of the IWS algorithm.

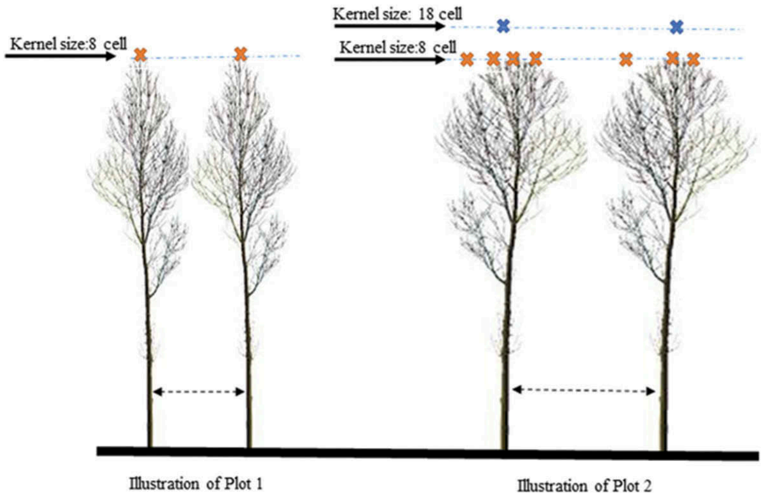

Figure 6. Example to illustrate the potential problems of identifying tree heights using different kernel radius sizes in forests with different tree shapes and structure for Plots 1 and 2.

were approximated to the nearest integer number of pixels. Among the several processing types we tested, in different variances of radius by using circular-shaped areas, we obtain the best results by setting a radius of eight-cell units within a kernel range $rm \in \{1, 2, 3, 4, 6, 8\ldots.18\}$ for Plot 1 and 18-cell radius for Plot 2, respectively. We hypothesized that different kernel radii were necessary for plots because the canopy structure of the trees of plot 2 was more circular; when we applied the same eight-cell kernel radius, similar to that in Plot 1, multiple pixels were identified as a treetop; thus, we increased the filtering value to identify a single treetop. Plot 2 trees were older and taller compared with those in Plot 1, which produced more oval/spherical shapes, unlike Plot 1 trees, which had more conical crown shapes (see Figure 6).

Focal statistics is a filtering tool that we used to identify the treetop location, based on the maximum pixel value in each kernel. Then we extracted the common pixel values, derived from the process of the focal statistics tool together with the CHM, to determine the positions of the highest pixel values (tree positions). For each input cell location, focal statistics calculate a statistic of the values in the form of weights within a specified neighbourhood around it; it returns Mean, Standard Deviation, or Sum values as needed. To match the pixel values from CHM and the focal statistic result, we used equation (1):

$$\mathrm{Con}('\mathrm{CHM}' == '\text{focal statistics result}', 1). \tag{1}$$

Conditional tool (Con) performs a conditional if/else evaluation on each of the input cells of an input raster and returns back the binary value of 0 (for non-data) or 1 (for data value). The return value was the value when the CHM value equalled the focal statistics output (raster).

When we tried to match the efficiency of tree positions obtained from the UAV platform with the field measurements, we detected a slight spatial inaccuracy (tilted positions of trees resulted from the UAV) caused by the lack of precision of the on-board

GPS. To solve this problem, we used the azimuth and horizontal distances, measured in the field to identify the X, Y tree positions. For each plot, we georeferenced four tree point positions, in order to match the tree positions acquired from the UAV with those of the terrestrial data.

2.6. *Calculation of crown diameters*

For individual tree canopy delineation, we used the method of IWS, as proposed by Edson and Wing (2011). We used the IWS method in ArcGIS 10.3.1 (ESRI) mainly because of its ability to delineate distinct tree entities, especially in relatively closed forest canopy structures. To implement the IWS, we inverted the CHM raster surface, whereby treetops become 'ponds' and tree branches/crowns become watersheds. Using the inverted CHM, we then created the flow direction layer to create individual hydrologic drainage basins (Wannasiri et al. 2013), which identified the crown delineations in the form of a raster layer. However, this layer contained large gaps located between tree crowns. To identify the tree crowns for delineation, we used the Boolean layer of the CHM to reclassify the new output into two different categories. For Plot 1, the first category identified all of the pixels that had values greater than 17 m (pixel values = 1) and the second category identified all pixel values less than 17 m, including gap areas (values = 0). We determined this threshold value by testing a range of different height values (14–19 m); this range was based on the shortest trees in the plot and the ground field height measurements. Plot 2 had taller trees; thus, we had to increase the threshold value to 20 m. To identify all the gap areas in the plots, we multiplied the result of the Boolean layers with the basin layer.

Finally, we converted the inverted CHM to polygons, to provide a layer for measuring the crown diameters, as shown in Figure 5(*b*). Shapefiles were exported as polygons to delineate tree crowns; we used the QGis V 2.12.0 (®Free–Open Source Software Foundation, Inc., Boston, MA, USA) package to measure the crown diameters. We established the centre for each polygon and we converted the polygons to lines and then line to points to assign the points to the periphery of each polygon; we then used the distance tool to find the diameter of the crown. To preserve the integrity of our data, all GIS measurements of the crown diameters were performed in the same manner as the field data collection when applicable, e.g. orientation of diameter measurements (north–south and east–west).

2.7. *Statistics and validation of data*

To compare the estimates of tree height and crown diameter from UAV flights with field measurements, we used a tree-level approach. All statistical analyses were conducted in MATLAB (MathWorks®), Inc. and Excel (Microsoft® office). We used linear regression analysis to model the relationship between the estimated and measured variables and we calculated the R-squared as a metric for accuracy. Additionally, box-and-whisker plots were used to illustrate the variance for the measured and estimated variables. To determine whether the estimated heights and crown diameters were significantly different from the measured values, we compared the mean of differences using confidence intervals and paired *t*-tests. We also calculated the residuals as the difference between individual tree parameters estimated from the CHM and the field measurements. As a better illustration for the distribution of error around the mean of data (how close predictions are to the eventual outcomes), we also computed the mean absolute error (MAE) and then we evaluated the residuals for each plot for both measured and estimated variables. The MAE is given by Equation (2) as follows:

$$\mathrm{MAE} = \frac{1}{n}\sum_{i=1}^{n}|f_i - y_i| = \frac{1}{n}\sum_{i=1}^{n}|e_i|. \tag{2}$$

As the name suggests, the MAE is an average of the absolute errors, $|\mathrm{e_i}| = |f_i - y_i|$ where f_i is the prediction and y_i is the true value.

3. Results

3.1. *Tree height and crown estimation*

Plot 1 had 49 trees and Plot 2 had 39 trees; the height measures (terrestrial data) and crown diameter estimations (UAV data) of each plot are summarized in Table 1. In Plot 1, the median and mean height values indicate UAV data underestimated tree heights (see Table 1) and overestimated crown diameters; in Plot 2, both tree heights and crown diameters were overestimated.

Linear regression (see Figure 7) exhibited a strong relationship between the estimated and measured tree heights in Plot 1 ($R^2 = 0.75$) and Plot 2 ($R^2 = 0.72$). Similarly, the estimated crown diameters in Plot 1 ($R^2 = 0.63$) and Plot 2 ($R^2 = 0.85$) also showed good fit with the estimated values (see Figure 10). In general, taking a better look (see Figure 8; Figure 11) for both tree variables and both study areas and in accordance with the above results, we can point out that we have wider ranges of variation of mean values between the estimated values compared with the terrestrial measurements in case of height. On the contrary, exception is the means of crown variable for both plots (see Table 3).

To improve the regression model, we also calculated the residuals. More specifically, in Plot 1, the MAE of height was 2.62 m, and the height accuracy was lower in Plot 2 with MAE of height equal to 2.88 m (see Figure 9). For crown diameter, the results were similar to the higher accuracy in Plot 1 (MAE = 0.73 m) compared with Plot 2 (MAE = 0.80 m) (see Figure 12). The estimated and measured tree heights and crown diameters in Plot 1 had a mean difference of 1.55 m and –0.42 m, respectively, whereas in Plot 2 the mean differences were –2.35 m and –0.70 m, respectively (see Figure 13; see Table 5).

Table 1. Statistics of the measured and estimated height variables for the two study areas at the tree level.

	Plot 1		Plot 2	
	Measured tree height (m)	Estimated height (UAV) (m)	Measured tree height (m)	Estimated height (UAV) (m)
H min	13.3	16.2	17.9	20.4
H Q1	21.3	20.8	24.5	27.5
H median	24.2	22.5	26.7	29.9
H Q3	28.1	24.1	30.1	31.2
H max	34.4	30.1	32.7	34.8
H mean	24.2	22.3	27.0	29.4

CD: crown diameter (min, max, and median values); Q: quartiles (Q1:25% (lower) – 50% (median) – Q3: 25% (upper)).

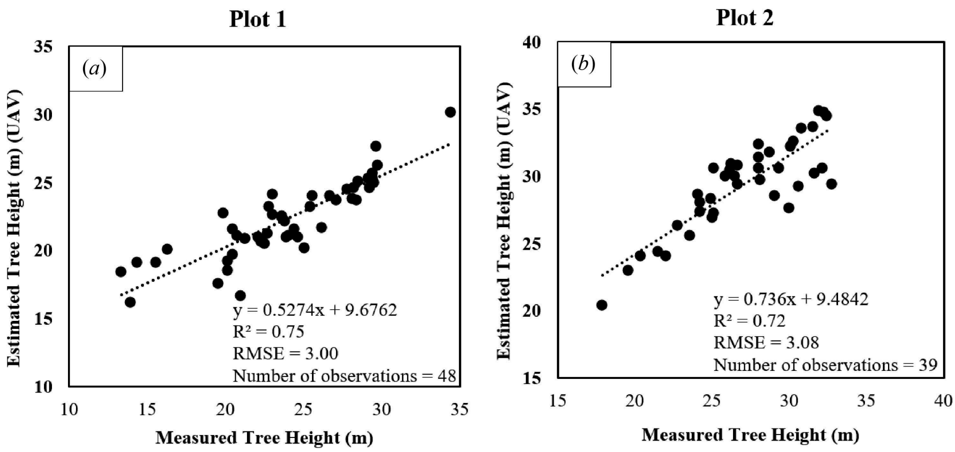

Figure 7. Linear regression models of the estimated (UAV) and measured (ground truth) heights for Plot 1 (a) and Plot 2 (b).

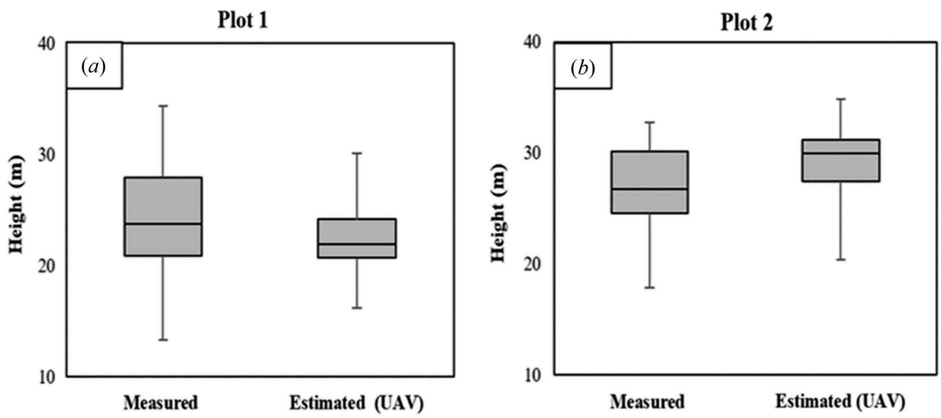

Figure 8. Box-and-whisker plots of the measured and estimated height variables for both study areas based on 48 trees in Plot 1 (a) and 39 trees in Plot 2 (b).

The root mean square error (RMSE) (m) for height (see Table 2) in Plot 1 was 3.00 m and it was 3.08 m in Plot 2, whereas the crown projection RMSE (m) in Plot 1, 0.82 m, was obviously lower than the RMSE (m) of 1.04 in plot 2 (see Table 4). However, because the plots had different means, we wanted to normalize the RMSE by dividing the RMSE by the mean of the plots to calculate the RMSE% for comparing the accuracy between the plots.

RMSE% for height (see Table 2) and crown diameter (see Table 4) evaluation varied by plot, ranging from 11.42 to 18.56. Particularly, in Plot 1 the estimation of height and crown diameter RMSE% was similar, 12.62 and 14.29, respectively, but for Plot 2 the RMSE% were quite different for height (11.42) and crown diameter (18.56) estimates. In both plots, the estimated and measured values for height and crown diameter were similar, as supported by the R^2 values of the linear regression models.

According to the *t*-test result, the absolute value of the *t*-statistics for the estimated heights and crown projections in both plots exceeded the critical values (see Tables 2

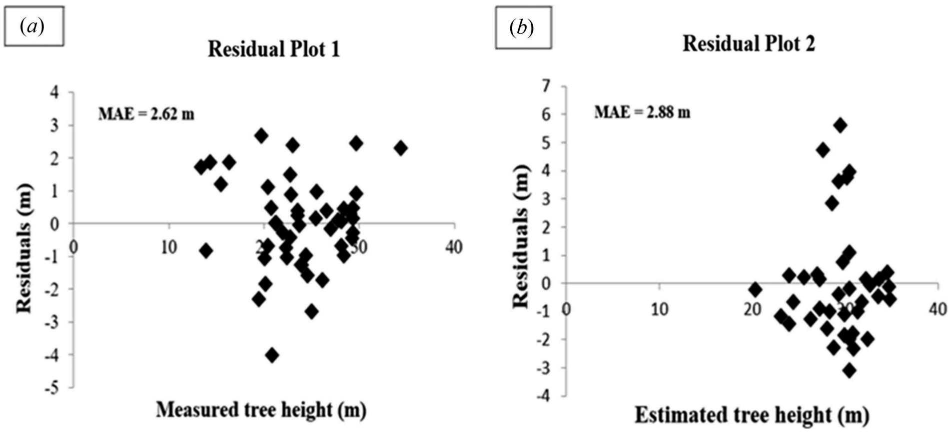

Figure 9. Residual plots displaying the distribution of errors around the mean estimated height for Plot 1 (a) and Plot 2 (b).

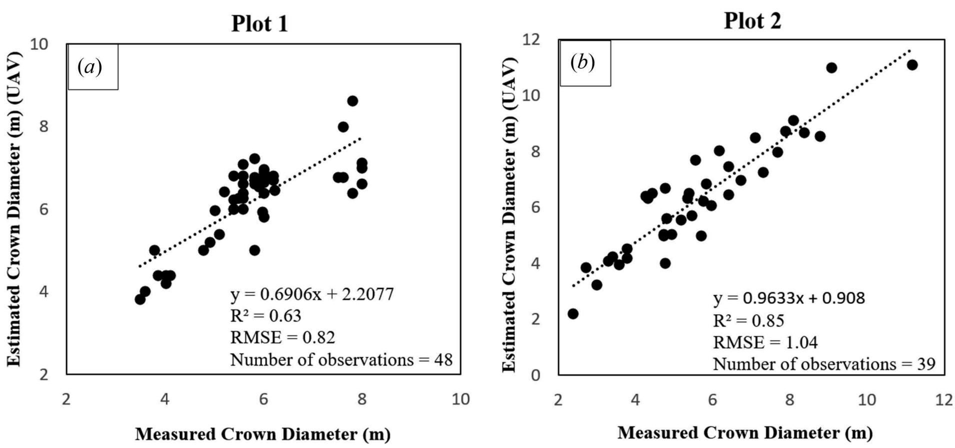

Figure 10. Linear regression models of the estimated (UAV) and measured (ground truth) crown diameters for Plot 1 (a) and Plot 2 (b).

and 4); based on this result, we rejected the null hypothesis and concluded that the two plot means were different at a 0.05 significance level.

4. Discussion

Low-altitude UAV imagery may be used to systematically observe forest canopy height (Baltsavias et al. 2008; Dandois and Ellis 2010). Structural forest attributes are commonly extracted from the CHM by means of regression models to predict tree features for forest inventories (e.g. descriptive statistic of the CHM on a particular area) (Næsset, 2002; Næsset et al. 2004). The practical outcomes of CHMs, in combination with terrestrial measurements, are the prediction of forest attributes of interest, e.g. crown diameter and height estimation.

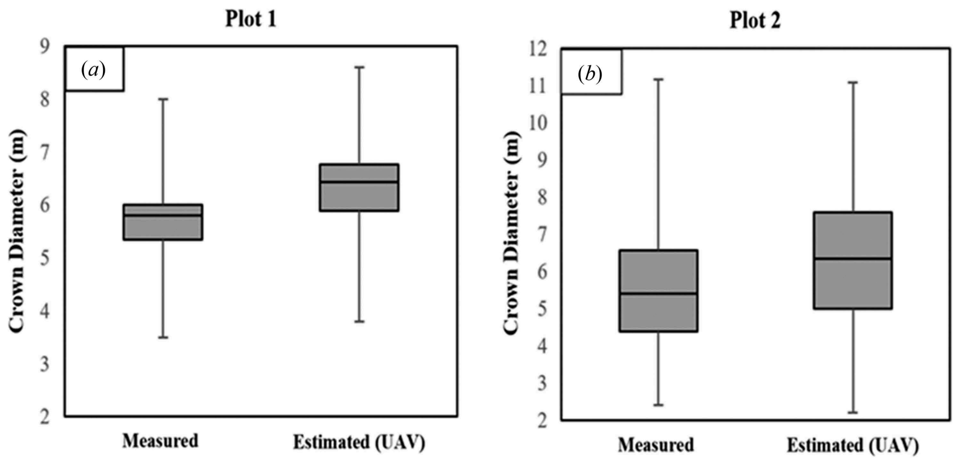

Figure 11. Box-and-whisker plots of both measured and estimated crown diameters for both study areas based on 48 trees in Plot 1 (a) and 39 trees in Plot 2 (b).

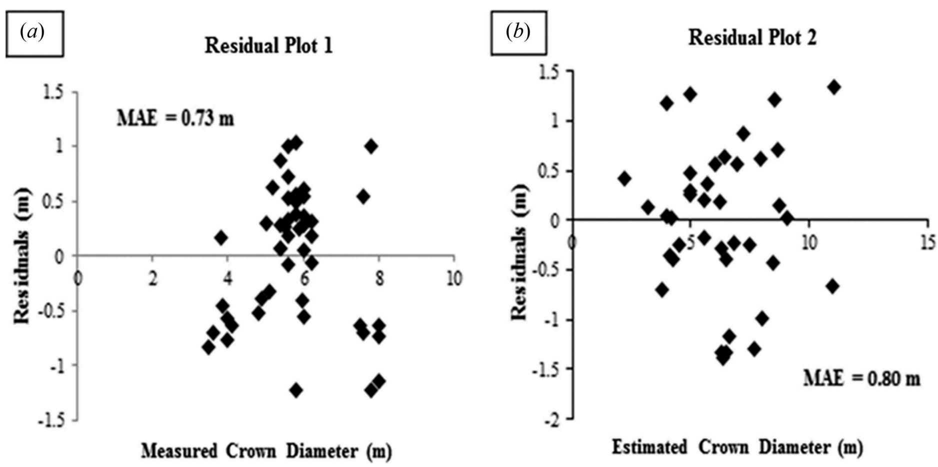

Figure 12. Residual plots displaying the distribution of errors around the mean estimated crown diameter for Plot 1 (a) and Plot 2 (b).

Based on the *t*-test results, we rejected the null hypothesis because the means for both plots were different at a 0.05 significance level. Although the differences between means were significant according to paired *t*-tests, the error of estimates from the UAV was relatively small and therefore considered acceptable. However, low accuracy, especially crown diameter, was observed in both plots (RMSE % = 14.29), but with lower accuracy in Plot 2 (RMSE% = 18.56) (see Table 4). This can be partially explained by the combination of pixels from gap areas with the pixels of 'real' crown area, which can cause overestimation of crown diameter (Diaz -Varela et al. 2015).

Absolute RMSE (m) showed a higher agreement for crown diameter than height for both Plot 1 (0.82 m) and Plot 2 (1.04 m). Estimates of height and crown diameter had an RMSE%

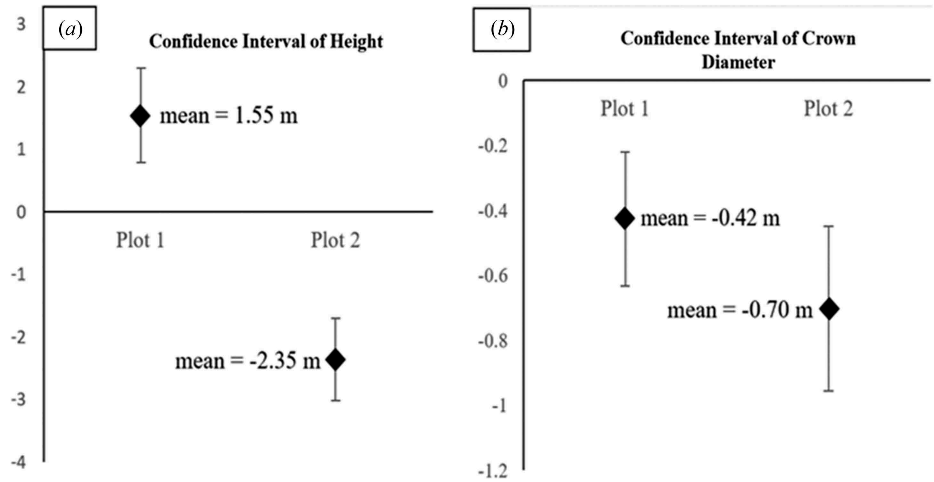

Figure 13. The mean of differences for the estimated–measured tree heights and crown diameters for both plots.

Table 2. Statistical summary of height estimates for Plots 1 and 2.

	RMSE (m)	RMSE %	Bias	Bias %	MAE (m)	P(T ≤ t) two-tail *t*-test	t Critical two-tail *t*-test	t Stat	*p*-Value	df
Plot 1	3.00	12.62	−1.55	−6.99	2.62	0.15	2.01	4.14	0.00	47
Plot 2	3.08	11.42	2.35	8.02	2.88	0.00	2.02	7.27	0.00	38

RMSE: root mean square error; RMSE%: root mean square error percentage; MAE: mean absolute error; bias; bias%: two-tailed *t*-test; *t*-statistic; df: degrees of freedom.

Table 3. Statistics of the measured and estimated crown diameter variables for the two study sites at the tree level.

	Plot 1		Plot 2	
	Measured CD (m)	Estimated CD (UAV) (m)	Measured CD (m)	Estimated CD (UAV) (m)
CD min	3.5	3.8	2.4	2.2
CD Q1	5.4	5.9	4.4	5.0
CD median	5.8	6.4	5.4	6.3
CD Q3	6.0	6.8	6.6	7.6
CD max	8.0	8.6	11.2	11.1
CD mean	5.7	6.2	5.6	6.3

CD: crown diameter (min, max, and median values); Q: quartiles (Q1:25% (lower) – 50% (median) – Q3: 25% (upper)).

Table 4. Statistical summary of crown diameter estimates for Plots 1 and 2.

	RMSE (m)	RMSE %	Bias	Bias%	MAE (m)	P(T ≤ t) two-tail t-test	t Critical two-tail *t*-test	t Stat	*p*-Value	df
Plot 1	0.82	14.29	0.43	6.92	0.73	0.00	2.01	4.17	0.00	47
Plot 2	1.04	18.56	0.70	11.11	0.80	0.00	2.02	5.61	0.00	38

RMSE: root mean square error; RMSE%: root mean square error percentage; MAE: mean absolute error; bias; bias%, two-tailed *t*-test; *t*-statistic; df: degrees of freedom.

lower than 20 for most results. Zarco-Tejada et al. (2014) compared the height data retrieved from high-resolution images and ground measurements; similarly, they determined that the RMSE% ranged between 10 and 13, depending on the study area. In Plot 2, where the

Table 5. Statistical summary table displays the confidence interval of mean value of differences, standard deviation, the size of the sample plots (total number of observations), the confidence interval as an estimated range of values, and the two-sided confidence limits for both plots.

						Confidence Range (m)	
	Number of Plots	Mean (m)	Standard Dev. (m)	Sample Size	Confidence Interval (m)	Upper Bound	Lower Bound
Height	1	1.55	2.59	48	2.04	0.75	0.75
	2	−2.35	2.02	39	2.02	0.65	0.65
Crown Diameter	1	−0.42	0.71	48	2.04	0.21	0.21
	2	−0.70	0.78	39	2.02	0.25	0.25

discontinuous canopy yielded a higher percentage of gap areas, RMSE% for crown diameter was 18.56, which is still acceptable when compared with errors that may occur with field measurements (Diaz-Varela et al. 2015; Paulus et al. 2014; Paproki et al. 2012).

Height and crown diameter estimates for Plot 1 were closer to the measured variables (see Table 5; see Figure 13). In addition, the confidence intervals indicated that the mean of the estimated crown diameters for both plots was significantly more similar than the estimated height variables, which were significantly different (underestimation of heights for Plot 1 and overestimation of height for Plot 2). These findings may be attributable to the differences in heights of trees (mean Plot 1 = 24.2 m, mean Plot 2 = 27 m) and similarity of crown diameters (mean Plot 1 = 5.7 m, mean Plot 2 = 5.6 m) in the two plots.

Although the proposed approach caused some systematic errors related to image smoothing, it can result in low and acceptable errors, which can be useful for monitoring the variation of forest attributes relevant to forest management (Diaz-Varela et al. 2015).

5. Conclusions

In this study, we tested the performance of tree detection algorithms based on UAV SfM point clouds, and we assessed the accuracy of tree height and diameter measurements derived from both point clouds. We reconstructed 3D forest canopy models based on SfM techniques to evaluate tree height and crown diameter. The proposed workflow consists of UAV image acquisition data from an RGB camera, processing of the point cloud, construction of the CHM from DSM and DEM, and GIS processing-analyses and watershed algorithm application for the calculation of tree variables. Many studies have previously treated estimates of tree parameters, such as tree crown delineation and treetop detection, as two separate procedures (Wang, Gong, and Biging 2004). In fact, tree crown boundaries and treetop detection should be considered as continuous processes; the derivation of one aspect can assist in the solution of the other. However, these assumptions have some limitations and can only be applied to forest structures with more homogeneous crown structures, especially with large crowns, because otherwise several local maxima can be found for a single crown surface. In addition, the location of the treetop is the basis for extracting tree height and delineating the crown projection area. We found that the choice of filters for smoothing the CHM has a significant influence on the detection of treetops. Therefore, the decision on how to determine the treetop location is critical and it is largely based on the knowledge and experience we have about the structure of the forest. It is also worth noting the fact that estimations from photos tend to show a slightly higher dispersion of data, which could be associated with image artefacts related to data acquisition, errors during processing, or human factors during ground measurements. In fact, the nadir view of the tree crown, taken from remote sensors in the height estimation, could account for tree irregularities, which may go unidentified by individuals taking ground measurements (Moorthy et al. 2011).

To potentially improve the results of the 3D image reconstruction model and ensure the integrity of the results based on CHM, we used four ground reference points, measured with RTK GPS. In this study, instead of using a more sophisticated approach for treetop estimates, we simply tested and used threshold values applied on morphological filters to remove non-treetop maxima. Concerning the estimation of crown diameters, large gaps between the trees within our study area produced an inaccurate delineation of solitary trees using IWS. To correct the model and leave only the tree crowns for delineation, we excluded the areas with elevation lower than 17 m in the layer of CHM for Plot 1, and 20 m in the same layer for Plot 2 (because the shortest trees found in Plot 1 and Plot 2 were 17 m and 20 m, respectively); this produced the best fitted delineation for our trees. Pixels with high elevations may be the result of bushes or leaf present in the gap areas, a factor that can result in the misidentification of tree crowns.

As a general conclusion regarding the performance of remote sensing versus field measurements, we can say that the comparison between reference field measurements and remote-sensing estimation of crown parameters confirmed the performance of the workflow applied as a quick and effective alternative to characterize forest tree crown diameters. Finally, high accuracy of height and crown diameter estimates was produced for both plots; based on the RMSE% values comparing remote-sensing and field techniques, crown diameter appeared to be of lower accuracy for both plots, but the results were considered satisfactory.

Acknowledgements

This research was funded by the Ministry of Finance of the Czech Republic, grant of Iceland, Liechtenstein and Norway 'Frameworks and possibilities of forest adaptation measures and strategies connected with climate change' No. EHP-CZ02- OV-1-019-2014, and the Internal Grant Agency (IGA) of the Faculty of Forestry and Wood Sciences at the Czech University of Life Sciences in Prague (No. B07/15). The authors would also like to acknowledge Dr Přemysl Janata of the Mendel University of Brno for his support and participation in the field campaign and measurements.

Disclosure statement

The authors declare no conflict of interest.

Funding

This work was supported by the Ministry of Finance of the Czech Republic, grant of Iceland, Liechtenstein and Norway; Frameworks and possibilities of forest adaptation measures and strategies connected with climate change [EHP-CZ02- OV-1-019-2014]; Internal Grant Agency; Forestry and Wood Sciences at the Czech University of Life Sciences Prague [B07/15].

Author contributions

Dimitrios Panagiotidis, Azadeh Abdollahnejad, and Vasco Chiteculo collected the ground measurements. Dimitrios Panagiotidis and Azadeh Abdollahnejad wrote the manuscript, analysed the images, and made the data analyses and interpretations. Vasco Chiteculo elaborated and adjusted the figures and Peter Surový supervised the manuscript.

References

Baltsavias, E., A. Gruen, H. Eisenbeiss, L. Zhang, and L. T. Waser. 2008. "High-Quality Image Matching and Automated Generation of 3D Tree Models." *International Journal of Remote Sensing* 29 (5): 1243–1259. doi:10.1080/01431160701736513.

Bodluc, P., K. Lowell, and G. Edwards. 1999. "Automated Estimation of Localized Forest Volumes from Large-Scale Aerial Photographs and Ancillary Cartographic Information in a Boreal Forest." *International Journal of Remote Sensing* 20 (18): 3611–3624. doi:10.1080/014311699211237.

Bortolot, Z. 2006. "Using Tree Clusters to Derive Forest Properties from Small Footprint Lidar Data." *Photogrammetric Engineering & Remote Sensing* 72: 1389–1397. doi:10.14358/PERS.72.12.1389.

Carleer, A. P., O. Debeir, and E. Wolff. 2005. "Assessment of Very High Spatial Resolution Satellite Image Segmentations." *Photogrammetric Engineering & Remote Sensing* 71 (11): 1285–1294. doi:10.14358/PERS.71.11.1285.

Chen, Q., D. D. Baldocchi, P. Gong, and M. Kelly. 2006. "Isolating Individual Trees in a Savanna Woodland Using Small Footprint Lidar Data." *Photogrammetric Engineering & Remote Sensing* 72: 923–932. doi:10.14358/PERS.72.8.923.

Dandois, J. P., and E. C. Ellis. 2010. "Remote Sensing of Vegetation Structure Using Computer Vision." *Remote Sensing* 2 (4): 1157–1176. doi:10.3390/rs2041157.

Dandois, J. P., and E. C. Ellis. 2013. "High Spatial Resolution Three-Dimensional Mapping of Vegetation Spectral Dynamics Using Computer Vision." *Remote Sensing of Environment* 136 (136): 259–276. doi:10.1016/j.rse.2013.04.005.

Diaz-Varela, R., R. De La Rosa, L. Leon, P. J. Zarco-Tejada, and J. Pablo. 2015. "High-Resolution Airborne UAV Imagery to Assess Olive Tree Crown Parameters Using 3D Photo Reconstruction: Application in Breeding Trials." *Remote Sensing* 7: 4213–4232. doi:10.3390/rs70404213.

Diaz-Varela, R. A., P. J. Zarco-Tejada, V. Angileri, and P. Loudjani. 2014. "Automatic Identification of Agricultural Terraces through Object-Oriented Analysis of Very High Resolution Dsms and Multispectral Imagery Obtained from an Unmanned Aerial Vehicle." *Journal of Environmental Management* 134 (134): 117–126. doi:10.1016/j.jenvman.2014.01.006.

Dralle, K., and M. Rudemo. 1996. "Stem Number Estimation by Kernel Smoothing of Aerial Photos." *Canadian Journal of Forest Research-Revue* 26 (7): 1228–1236. Canadienne De Recherche Forestiere. doi:10.1139/x26-137

Edson, C., and M. G. Wing. 2011. "Airborne Light Detection and Ranging (Lidar) for Individual Tree Stem Location, Height, and Biomass Measurements." *Remote Sensing* 3: 2494–2528. doi:10.3390/rs3112494.

Falkowski, M. J., A. M. S. Smith, A. T. Hudak, P. E. Gessler, L. A. Vierling, and N. L. Crookston. 2006. "Automated Estimation of Individual Conifer Tree Height and Crown Diameter via Two-Dimensional Spatial Wavelet Analysis of Lidar Data." *Canadian Journal of Remote Sensing* 32: 153–161. doi:10.5589/m06-005.

Fritz, A., T. Kattenborn, and B. Koch. 2013. "UAV-Based Photogrammetric Point Clouds—Tree Stem Mapping in Open Stands in Comparison to Terrestrial Laser Scanner Point Clouds." *International Archives of Photogrammetry, Remote Sensing & Spatial Information Sciences* XL-1/W2: 141–146. doi:10.5194/isprsarchives-XL-1-W2-141-2013.

Gini, R., D. Passoni, L. Pinto, and G. Sona. 2014. "Use of Unmanned Aerial Systems for Multispectral Survey and Tree Classification: A Test in A Park Area of Northern Italy." *European Journal of Remote Sensing* 2014 (47): 251–269. doi:10.5721/EuJRS20144716.

HAGLÖF SWEDEN, 2002, Vertex III and Transponder T3 Manual (English). Accessed 22 October 2003. http://www.forestrytools.com.au/VertexIII%20users%20guide.pdf

James, M. R., and S. Robson. 2012. "Straight Forward Reconstruction of 3D Surfaces and Topography with a Camera: Accuracy and Geoscience Application." *Journal of Geophysical Research* 2012: 117.

Kalliovirta, J., and T. Tokola. 2005. "Functions for Estimating Stem Diameter and Tree Age Using Tree Height, Crown Width and Existing Stand Database Information." *Silva Fennica* 39 (2): 227–248. doi:10.14214/sf.386.

Koch, B., U. Heyder, and H. Weinacker. 2006. "Detection of Individual Tree Crowns in Airborne Lidar Data." *Photogrammetric Engineering & Remote Sensing* 72: 357–363. doi:10.14358/PERS.72.4.357.

Küng, O., C. Strecha, A. Beyeler, J. C. Zufferey, D. Floreano, P. Fua, and F. Gervaix. 2011. "The Accuracy of Automatic Photogrammetric Techniques on Ultra-Light UAV Imagery." *International Archives of Photogrammetry, Remote Sensing & Spatial Information Sciences* XXXVIII-1: 125–130.

Maltamo, M., K. Eerikainen, J. Pitkaken, J. Hyypa, and M. Vehmas. 2004. "Estimation of Timber Volume and Stem Density Based on Scanning Laser Altimetry and Expected Tree Size Distribution Functions." *Remote Sensing of Environment* 90: 319–330. doi:10.1016/j.rse.2004.01.006.

Moorthy, I., J. R. Miller, J. A. J. Berni, P. Zarco-Tejada, B. Hu, and J. Chen. 2011. "Field Characterization of Olive (*Olea Europaea* L.) Tree Crown Architecture Using Terrestrial Laser Scanning Data." *Agricultural & Forest Meteorology* 151 (2): 204–214. doi:10.1016/j.agrformet.2010.10.005.

Naesset, E. 2002. "Predicting Forest Stand Characteristics with Airborne Scanning Laser Using a Practical Two-Stage Procedure and Field Data." *Remote Sensing of Environment* 80 (1): 88–99. doi:10.1016/S0034-4257(01)00290-5.

Paproki, A., X. Sirault, S. Berry, R. Furbank, and J. Fripp. 2012. "A Novel Mesh Processing Based Technique for 3D Plant Analysis." *BMC Plant Biology* 12 (1): 63. doi:10.1186/1471-2229-12-63.

Paulus, S., J. Behmann, A. K. Mahlein, L. Plumer, and H. Kuhlmann. 2014. "Low-Cost 3D Systems: Suitable Tools for Plant Phenotyping." *Sensors* 14 (2): 3001–3018. doi:10.3390/s140203001.

Peckham, R. J., and J. Gyozo. 2007. *Development and Applications in a Policy Support Environment Series: Lecture Notes in Geoinformation and Cartography*. Germany: University of Heidelberg.

Persson, Å., J. Holmgren, and U. Soderman. 2002. "Detecting and Measuring Individual Trees Using Airborne Laser Scanning." *Photogrammetric Engineering and Remote Sensing* 68 (9): 925–932.

Pitkänen, J., M. Maltamo, J. Hyyppä, and X. Yu. 2004. Adaptive Methods for Individual Tree Detection on Airborne Laser Based Canopy Height Model. In: M. Theis, B. Koch, H. Spiecker, and H. Weinacker, eds. Proceedings of ISPRS Working Group VIII/2: "Laser-scanners for forest and landscape assessment". Germany: University of Freiburg; pp. 187–191.

Popescu, S. C. 2007. "Estimating Biomass of Individual Pine Trees Using Airborne Lidar." *Biomass and Bioenergy* 31: 646–655. doi:10.1016/j.biombioe.2007.06.022.

Popescu, S. C., R. H. Wynne, and R. F. Nelson. 2002. "Estimating Plot-Level Tree Heights with Lidar: Local Filtering with a Canopy Height Based Variable Window Size." *Computers and Electronics in Agriculture* 37: 71–95. doi:10.1016/S0168-1699(02)00121-7.

Popescu, S. C., R. H. Wynne, and R. F. Nelson. 2003. "Measuring Individual Tree Crown Diameter with Lidar and Assessing Its Influence on Estimating Forest Volume and Biomass." *Canadian Journal of Remote Sensing* 29: 564–577. doi:10.5589/m03-027.

Pyysalo, U., and H. Hyyppä. 2002. Reconstructing Tree Crowns from Laser Scanner Data for Feature Extraction. In *ISPRS Commission III, Symposium*, 13 September 2002. Graz, Austria. pp. 218–221.

Remondino, F., L. Barazzetti, F. Nex, M. Scaioni, and D. Sarazzi. 2011. "UAV Photogrammetry for Mapping and 3D Modeling–Current Status and Future Perspectives. International Archives of the Photogrammetry." *Remote Sensing and Spatial Information Sciences* 38: 25–31.

Shao, G., S. Zhao, and H. H. Shugart. 1996. *Forest Dynamics Modeling – Preliminary Explanations of Optimizing Management of Korean Pine Forests*, 159. Beijing: *Chinese Forestry Publishing House*.

Sona, G., L. Pinto, D. Pagliari, D. Passoni, and R. Gini. 2014. “Experimental Analysis of Different Software Packages for Orientation and Digital Surface Modelling from UAV Images.” *Earth Science Informatics* 7: 97–107. doi:10.1007/s12145-013-0142-2.

Turner, D., A. Lucieer, and C. Watson. 2012. “An Automated Technique for Generating Georectified Mosaics from Ultra-High Resolution Unmanned Aerial Vehicle (UAV) Imagery, Based on Structure from Motion (Sfm) Point Clouds.” *Remote Sensing* 4 (12): 1392–1410. doi:10.3390/rs4051392.

Wang, L., P. Gong, and G. S. Biging. 2004. “Individual Tree-Crown Delineation and Treetop Detection in High-Spatial-Resolution Aerial Imagery.” *Photogrammetric Engineering & Remote Sensing* 70: 351–357. doi:10.14358/PERS.70.3.351.

Wannasiri, W., M. Nagai, K. Honda, P. Santitamont, and P. Miphokasap. 2013. “Extraction of Mangrove Biophysical Parameters Using Airborne LIDAR.” *Remote Sensing* 5 (4): 1787–1808. doi:10.3390/rs5041787.

Waser, L. T., E. Baltsavias, K. Ecker, H. Eisenbeiss, C. Ginzler, M. Kuchler, P. Thee, and L. Zhang. 2008. “High-Resolution Digital Surface Models (Dsms) for Modelling Fractional Shrub/Tree Cover in a Mire Environment.” *International Journal of Remote Sensing* 29 (5): 1261–1276. doi:10.1080/01431160701736422.

Zarco-Tejada, P. J., R. Diaz-Varela, V. Angileri, and P. Loudjani. 2014. “Tree Height Quantification Using Very High Resolution Imagery Acquired from an Unmanned Aerial Vehicle (UAV) and Automatic 3D Photo-Reconstruction Methods.” *European Journal of Agronomy* 55 (55): 89–99. doi:10.1016/j.eja.2014.01.004.